High-intensity nanosecond photorefractive spatial solitons

Konstantin Kos and Gregory Salamo

Department of Physics, University of Arkansas, Fayetteville, Arkansas 72701

Mordechai Segev

Department of Electrical Engineering, Princeton University, Princeton, New Jersey 08544

Received January 15, 1998

We report the observation of high-intensity solitons in a bulk strontium barium niobate crystal. The solitons are observed by use of 8-ns optical pulses with optical intensities greater than 100 MW/cm^2. Each soliton forms and attains its minimum width after roughly ten pulses and reaches e^{-1} of the steady-state width after the first pulse. We find good agreement between experimental observations and theoretical predictions for the soliton existence curve. © 1998 Optical Society of America

OCIS codes: 160.5320, 230.1360, 060.5530.

Optical spatial solitons[1] are currently stimulating much interest because their existence has potential for applications such as beam steering, optical interconnects, and nonlinear optical devices that use one light beam to control another. Both bright[2] and dark[3] one-dimensional (1D) Kerr-type spatial solitons, along with their ability to guide and switch other light beams, have been demonstrated.[4,5] For the most part these demonstrations generally require high intensities in the megawatt range. Interestingly, although Kerr solitons form as a result of the presence of a refractive-index change that is proportional to the optical intensity, it is precisely this dependence that prevents the existence of stable two-dimensional (2D) bright Kerr solitons. Recently, a new type of spatial soliton[1] based on the photorefractive effect was predicted and observed both in a quasi-steady-state regime[2,3] and more recently in the steady-state regime.[4–10] Compared with those of Kerr[11–14] spatial solitons, the most distinctive features of photorefractive spatial solitons are that they are observed at low light intensities [in the milliwatts per square centimeter (mW/cm^2) range] and that robust trapping occurs in both transverse dimensions. Both of these attributes make photorefractive solitons attractive for applications and for fundamental studies involving the interaction between spatial solitons.[15–22]

One transverse-dimension theory of photorefractive screening solitons[5–7] predicts a universal relationship among the width of the soliton, the applied electric field, and the ratio of the soliton intensity to the sum of the equivalent dark irradiance and a uniform background intensity. We refer to this curve as the soliton existence curve. This curve is important because experiments show that considerable deviations (~20% or more) from the curve lead to instability and breakup of the soliton beam,[10,22] whereas much smaller deviations are typically tolerated and are arrested by the soliton stability properties. In the case of a low-intensity photorefractive soliton beam, i.e., a beam with an intensity in the mW/cm^2 to kW/cm^2 range, recent 1D experiments have known good agreement with this universal relationship.[10,20]

Although the low-intensity feature of photorefractive spatial solitons is attractive for applications, high-intensity (MW/cm^2 to GW/cm^2) photorefractive solitons are also interesting, since the speed with which the steady-state screening soliton forms is inversely proportional to the optical intensity. As we show below, solitons in strontium barium niobate (SBN) can form at nanosecond speeds for GW/cm^2 intensities, which implies that for photorefractive semiconductors, which have mobilities 100–1000 times larger than those of the photorefractive oxides, soliton formation should occur at picosecond time scales for similar intensities. For these intensities, however, the excited free-carrier density is no longer smaller than that of the acceptors, and the space-charge field is due both to the free carrier and to the ionized donor contributions.[7]

In this Letter we report what we believe to be the first experimental observation of high-intensity screening solitons, along with a comparison between experimental results and theoretical predictions. To work in the high-intensity regime, one must satisfy the requirement that $1/r \ll a(u_0{}^2 + 1) \ll 1$, where $r = N_d/N_A$, $a = s(I_{\text{dark}} + I_b)/\gamma N_d$, N_d is the total donor number density, N_A is the number density of negatively charged acceptors that compensate for the ionized donors, $u_0{}^2$ is the ratio of the soliton intensity to the sum of the dark and the background intensities, I_b is the background intensity (used to control the effective dark carrier density), I_{dark} is the dark intensity, s is the photoionization cross section, and γ is the recombination rate coefficient. In our case, bright high-intensity solitons in photorefractive SBN can be realized at incident intensities of the order of 100 MW/cm^2 on a background of $I_b \sim 10$ MW/cm^2, which results in free-electron densities (for $T \sim 300$ K) of 10^{17} cm^{-3} in the center of the soliton and 10^{16} cm^{-3} far from the center. For the experiment reported here, we used a crystal with $N_d \sim 10^{18}$ cm^{-3} and $N_A \sim 10^{15}$ cm^{-3} ($r = 10^3$ and $a \sim 0.1$).

For the experiment we used a Q-switched YAG laser to generate a high-intensity 8-ns second-harmonic pulse at 530 nm that was split into two beams. One beam acted as the soliton beam, and the second beam

0146-9592/98/131001-03$15.00/0

provided the background intensity. The background beam filled the entire crystal, and the soliton beam was focused with a cylindrical lens to 11 μm (FWHM) $\times$ 2 mm at the crystal entrance face. We used the cylindrical lens to observe a 1D soliton. That is, the beam was essentially infinite in extent in the vertical, or b, direction and 11 μm in the horizontal, or c direction. Both beams propagated along the crystalline a axis (for SBN $a = b$), and an electric field was applied along the c axis. The soliton beam was extraordinarily polarized, allowing us to take advantage of the crystal's large r_{33} electro-optic coefficient, and the background beam was ordinarily polarized, making it possible to select only the soliton beam for observation by use of a polarizer. In particular, the soliton beam was observed with an imaging lens to image and magnify the intensity distribution at the crystal entrance and exit faces. Figure 1 shows typical experimental results of the entrance intensity waveform, the exit intensity waveform without trapping (zero voltage), and the exit intensity waveform with trapping (when 1500 V were applied to the crystal between electrodes separated by 6 mm). The waveforms shown evolved from 8-ns pulses at an intensity of 100 MW/cm^2 after ten pulses.

Although it took ten pulses to reach the steady-state condition, the intensity of illumination during each pulse was in the high-intensity regime, and the beam diameter reached e^{-1} of its steady-state value during the first pulse. Moreover, the crystal dark current was so small that the measured beam diameter at the end of each pulse was found to be independent of the time between pulses over a range from 0.1 to 1000 s. For these two reasons, our crystal can be considered to be in effective illumination at 100-MW intensities for a period of 80 ns before the steady state is reached.

One-dimensional high-intensity screening solitons obey the normalized nonlinear wave equation[7]

$$\mathrm{d}^2u/\mathrm{d}\xi^2 + \delta u - u/(1 + u^2)^{1/2} = 0\,, \qquad (1)$$

where $u(\xi)$ is the soliton amplitude (as a function of the transverse coordinate ξ) divided by the square root of the sum of the background and the dark intensities; u_0 is $u(\xi = 0)$; $\delta = 2[(u_0{}^2 + 1)^{1/2} - 1]/u_0{}^2$; and $\xi = x/d$, where we have $d = (k^2 n_b{}^2 r_{\mathrm{eff}} V/l)^{-1/2}$, $k = 2n_b/\lambda$, λ is the free-space wavelength, n_b is the unperturbed refractive index, r_{eff} is the effective electro-optic coefficient for the geometry of propagation, V is the applied voltage, and l is the width of the crystal between the electrodes. We can integrate Eq. (1) numerically to obtain the spatial profile of the soliton and the FWHM of the intensity as a function of u_0, which is the soliton existence curve. These results are shown in Fig. 2 (solid curve) for the range $0.1 \le u_0 \le 100$, along with the low-intensity case (dotted curve) for comparison. The difference in the two theoretical curves occurs because the change in the refractive index, Δn, is proportional to $(1 + u^2)^{-1/2}$ for the high-intensity solitons shown in Fig. 2, whereas for low-intensity screening solitons Δn is proportional to $(1 + u^2)^{-1}$. Our experimental results with 1D solitons of the same width and wavelength and in the same crystal for both low- and high-intensity solitons are marked by the open and filled squares, respectively, in Fig. 2. It is apparent that there is good agreement between experiments and theory for both the high- and the low-intensity cases. The predominant reason for the discrepancy is that the background beam is slightly guided by the refractive-index change induced by the soliton[10] (since r_{13} is not zero) rather than maintaining a constant value across the beam as is assumed theoretically.

Although both low- and the high-intensity bright screening solitons depend on the ratio of the soliton peak intensity to the background plus the dark intensity, there are three striking differences between the high- and low-intensity regimes. The first is that the lowest voltage required for trapping a bright soliton is obtained when this ratio is $\approx$2.4 in the low-intensity regime and $\approx$5.5 in the high-intensity regime. Indeed, in our experiments this most favorable point in the high-intensity regime is shifted toward higher intensity ratio values than those for the low-intensity curve. Second, since the dark irradiance is extremely low in SBN, i.e., mW/cm^2 (or less), the low-intensity regime can, in principle, be reached without the use of a background beam ($I_b = 0$). For the high-intensity case, however, the background beam is essential and is many orders of magnitude higher than the dark intensity. Third, the slope of the low-intensity curve is significantly greater than the corresponding slope

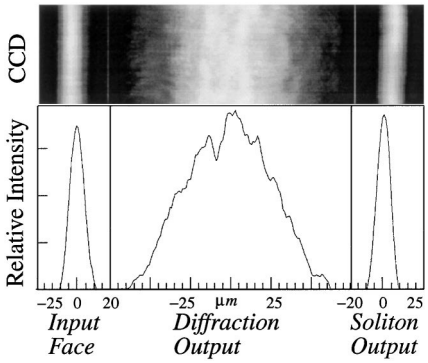

Fig. 1. Horizontal intensity profiles at the crystal entrance face (left), at the crystal exit face, without an applied trapping field (center), and for a 1D soliton at the crystal exit face, with applied trapping voltage (right).

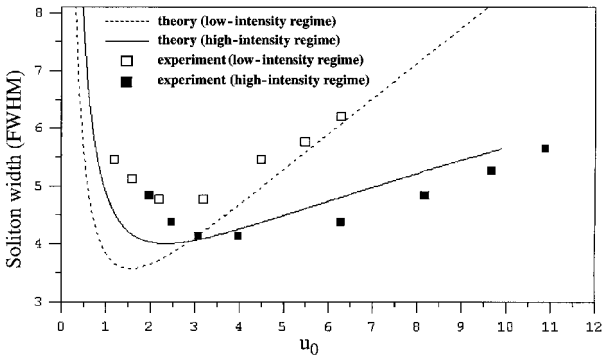

Fig. 2. Widths (FWHM of the intensity) of 1D low- and high-intensity solitons as a function of the soliton peak intensity to the background intensity plus the dark intensity ratio, along with corresponding experimental data.

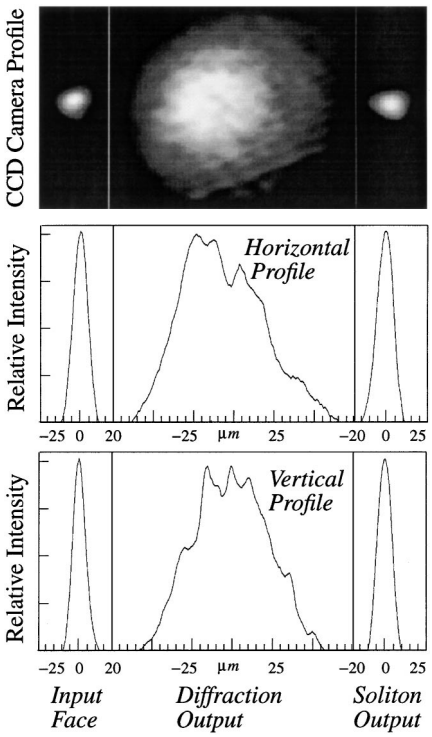

Fig. 3. Horizontal and vertical intensity profiles at the crystal entrance face (left), at the crystal exit face, without applied trapping field (center), and for a 2D soliton at the crystal exit face, with applied trapping voltage (right).

for the high-intensity regime when $u_0^2 > 5$. This difference in slope leads, for example, to a soliton width in the high-intensity regime that is substantially lower than the corresponding soliton width in the low-intensity regime for a given intensity ratio. As seen in Fig. 2, this difference in slope is one of the striking differentiating features supported by the experimental results presented in this Letter.

Since precise theoretical predictions exist only for the 1D case, a 1D experiment was necessary for a valid comparison with theory. However, 2D high-intensity screening solitons are even more interesting, both for fundamental reasons and for applications. Figure 3 shows typical results for a 2D high-intensity experiment for the same conditions as those in the 1D experiment. Although it is not shown in Fig. 2, the slope of the experimental 2D high-intensity existence curve when $u_0^2 > 5$ was identical to that in the 1D high-intensity case.

In conclusion, we have demonstrated that screening spatial solitons in both one and two dimensions are observable with 8-ns megawatt optical pulses. The behavior of these high-intensity screening solitons differs significantly from that of previously reported low-intensity cw screening spatial solitons but is accurately described by their existence curve.

References

1. R. Y. Chiao, E. Garmire, and C. H. Townes, Phys. Rev. Lett. **13,** 479 (1964).
2. M. Segev, B. Crosignani, A. Yariv, and B. Fischer, Phys. Rev. Lett. **68,** 923 (1992).
3. G. Duree, J. L. Shultz, G. Salamo, M. Segev, A. Yariv, B. Crosignani, P. DiPorto, E. Sharp, and R. R. Neurgaonkar, Phys. Rev. Lett. **71,** 533 (1993); **74,** 1978 (1995).
4. G. C. Valley, M. Segev, B. Crosignani, A. Yariv, M. M. Fejer, and M. Bashaw, Phys. Rev. A **50,** R4457 (1994); M. Taya, M. Bashaw, M. M. Fejer, M. Segev, and G. C. Valley, **52,** 3095 (1995).
5. M. Segev, G. C. Valley, B. Crosignani, P. DiPorto, and A. Yariv, Phys. Rev. Lett. **73,** 3211 (1994).
6. D. N. Christodoulides and M. I. Carvalho, J. Opt. Soc. Am. B **12,** 1628 (1995).
7. M. Segev, M. Shih, and G. C. Valley, J. Opt. Soc. Am. **13,** 706 (1996).
8. M. D. Iturbe-Castillo, P. A. Marquez-Aguilar, J. J. Sánchez-Mondragón, S. Stepanov, and V. Vysloukh, Appl. Phys. Lett. **64,** 408 (1994).
9. M. Shih, M. Segev, G. C. Valley, G. Salamo, B. Crosignani, and P. DiPorto, Electron. Lett. **31,** 826 (1995); M. Shih, P. Leach, M. Segev, M. H. Garrett, G. Salamo, and G. C. Valley, Opt. Lett. **21,** 324 (1996).
10. K. Kos, H. Ming, G. Salamo, M. Shih, M. Segev, and G. C. Valley, Phys. Rev. E **53,** R4330 (1996).
11. J. S. Aitchison, A. M. Weiner, Y. Silberberg, M. K. Oliver, J. L. Jackel, D. E. Leaird, E. M. Vogel, and P. W. E. Smith, Opt. Lett. **15,** 471 (1990).
12. G. A. Swartzlander, Jr., D. R. Anderson, J. J. Regan, H. Yin, and A. E. Kaplan, Phys. Rev. Lett. **66,** 1583 (1991).
13. R. De La Fuente, A. Barthelemy, and C. Froehly, Opt. Lett. **16,** 793 (1991).
14. B. Luther-Davies and Y. Xiaoping, Opt. Lett. **17,** 496 (1992).
15. M. Shih and M. Segev, Opt. Lett. **21,** 1538 (1996).
16. M. Shih, Z. Chen, M. Segev, T. H. Coskun, and D. N. Christodoulides, Appl. Phys. Lett. **69,** 4151 (1996).
17. M. Shih, M. Segev, and G. Salamo, Phys. Rev. Lett. **78,** 2551 (1997).
18. G. S. Garcia-Quirino, M. D. Iturbe-Castillo, V. A. Vysloukh, J. J. Sánchez-Mondragón, S. I. Stepanov, G. Lugo-Martinez, and G. E. Torres-Cisneros, Opt. Lett. **22,** 154 (1997).
19. W. Krolikowski and S. A. Holmstrom, Opt. Lett. **22,** 369 (1997).
20. H. Meng, G. Salamo, M. Shih, and M. Segev, Opt. Lett. **22,** 448 (1997).
21. D. N. Christodoulides, S. R. Singh, M. I. Carvalho, and M. Segev, Appl. Phys. Lett. **68,** 1763 (1996).
22. Z. Chen, M. Segev, T. Coskun, and D. N. Christodoulides, Opt. Lett. **21,** 1436 (1996).